

Dual-Responsive Janus Membrane by One-Step Laser Drilling for Underwater Bubble Selective Capture and Repelling

Sizhu Wu, Dong Meng, Chao Chen,* Lu-An Shi, Lili Zhou, Zhouchen Huang, Jiawen Li, Yanlei Hu, and Dong Wu*

Achieving the dynamic control of underwater gas bubbles (UGBs) on smart surfaces has aroused great attention for academic research and industrial applications. To date, developing a kind of stimuli-responsive porous membrane with asymmetric wettability which can be reversibly switched between Janus and non-Janus systems, unfortunately, has been rarely demonstrated. Here, a light/temperature-responsive Janus tapered-hole arrayed zinc foil (TAZF) is unfolded by combining one-step laser drilling and a subsequent heating which is successfully utilized for underwater bubble unidirectional transport, that is, bubble “diode.” Moreover, this TAZF can reversibly switch between Janus architecture and double-faced aerophobic by applying alternative heating and UV dispositions for selectively capturing or repelling bubbles. The underlying mechanism revealed by X-ray photoelectron spectroscopy spectrums is that the reversible graft and removal of hydroxyl (–OH) on the top surface of TAZF dominates the wettability conversion. The quantitative relationship among the UV and heating time and the water contact angle and the underwater bubble contact angle (UGBCA) is also studied. This work provides insight for designing smart surfaces applicable in fast bubble capture, transportation, collection, and gas/liquid separation.


Achieving the controllable transport of underwater gas bubbles (UGBs) is of great significance for academic research and industrial implement because of their potential applications in solar desalination,^[1] wastewater treatment,^[2] and minerals recovery.^[3] For example, selectively repelling bubbles can prevent the formation of a corrosive CO₂ solution on behalf of prolonging the lifetime of ocean vessels.^[4] In contrast, capturing bubbles can improve the gas diffusivity in aqueous media so as to enhancing the heat transfer efficiency in the ocean.^[5] Moreover, in a typical aeration process, capturing fine bubble can endow the microorganisms in sewage treatment ponds with sufficient dissolved oxygen, which renders profound significance for promoting the oxidation and decomposition of organic matter.^[6] In this regard, realizing the controllable transport of UGB is highly crucial for solving practical issues.

In the past decades, the unidirectional fluid transportation on the basis of asymmetric wettability of a Janus system has been extensively studied.^[7] Inspired by the mechanism of liquid self-transport, researchers have successfully realized the unidirectional transport of UGB by taking advantage of bubble “diode,” which is assembled by an aerophilic (AL) surface and another super-aerophobic (SAB) surface.^[8] UGB could readily pass through the Janus membrane from a SAB surface to an AL one, whereas it would be blocked in a reverse direction. For instance, Chen et al. successfully achieved the unidirectional penetration of UGBs via a Janus copper mesh, which was uniformly coated with hydrophilic TiO₂ nanoparticles on the top surface and modified with hydrophobic dodecane thiol on the bottom surface.^[9] Yong et al. realized selective passage of underwater bubbles by employing a Janus hierarchical through-microhole-array polydimethylsiloxane (PDMS) sheet. The upper surface of the Janus sheet is intrinsically hydrophobic and the lower surface is converted to hydrophilic by oxygen plasma treatment.^[10] Pei et al. manufactured an integrated Janus mesh with tunable aperture, whose top and bottom surfaces were carefully modified by chemical etching and competent for UGB antibuoyancy unidirectional transport.^[11] Recently, Yan et al. constructed a

Prof. S. Wu, D. Meng, L. Zhou
 School of Instrument Science and Opto-Electronics Engineering
 Hefei University of Technology
 Hefei 230009, China

Dr. C. Chen, Z. Huang, Prof. J. Li, Prof. Y. Hu, Prof. D. Wu
 CAS Key Laboratory of Mechanical Behavior and Design of Materials
 Department of Precision Machinery and Precision Instrumentation
 Key Laboratory of Precision Scientific Instrumentation of Anhui Higher Education Institutes
 University of Science and Technology of China
 Hefei 230026, China
 E-mail: chaoc11@ustc.edu.cn; dongwu@ustc.edu.cn

Dr. L.-A. Shi
 Division of Nanomaterials and Chemistry, Hefei National Laboratory for Physical Sciences at the Microscale, Collaborative Innovation Center of Suzhou Nano Science and Technology
 CAS Center for Excellence in Nanoscience
 Hefei Science Center of CAS, Department of Chemistry
 University of Science and Technology of China
 Hefei 230026, China

 The ORCID identification number(s) for the author(s) of this article can be found under <https://doi.org/10.1002/admi.201901176>.

DOI: 10.1002/admi.201901176

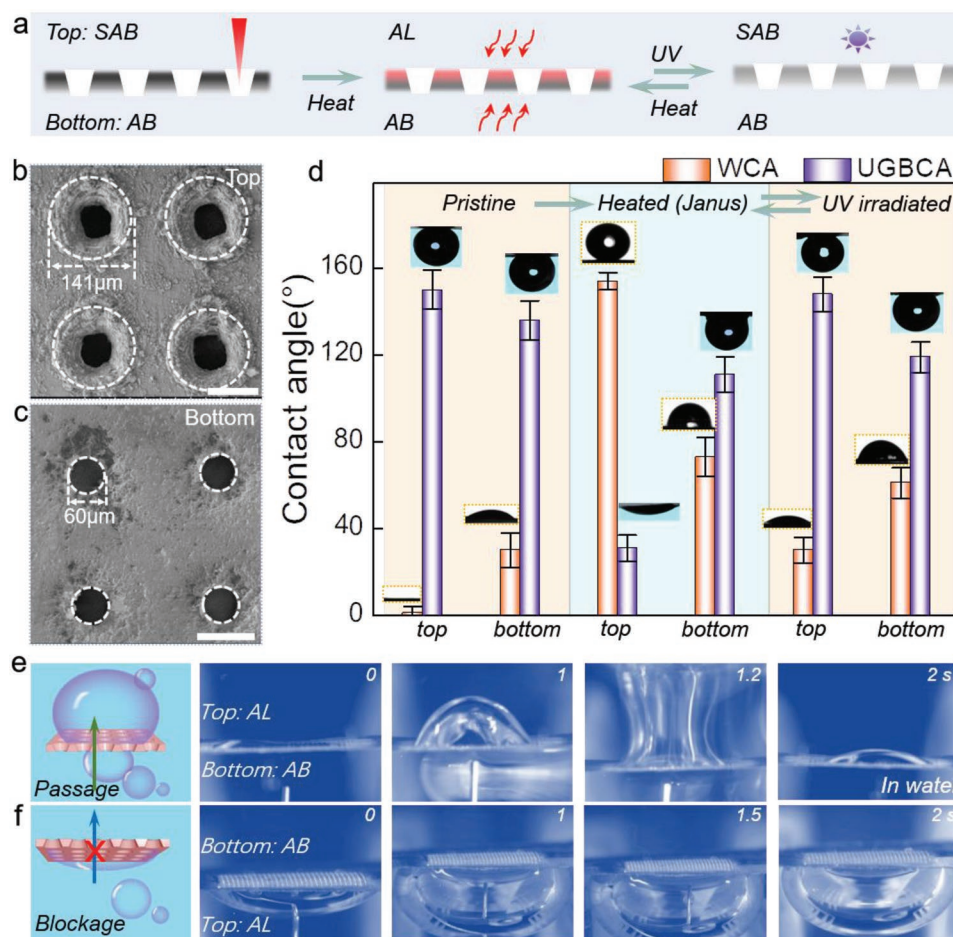


Figure 1. Facile fabrication of Janus TAZF and its reversible wettability. a) Schematic diagram for illustrating the wettability modulating strategy composed of one-step laser drilling (TAZF), heating (Heat-TAZF), UV irradiation (UV-TAZF), and re-heating (Re-Heat-TAZF), respectively. b,c) SEM images for the top and bottom surfaces of the resultant TAZF. d) Comparison of WCA and UGBCA for the top and bottom surfaces of TAZF, Heat-TAZF, UV-TAZF, and Re-Heat-TAZF, respectively. Dynamic clips for UGBs ejected from e) AB surface to AL one and f) AL surface to AB one of Heat-TAZF, respectively. The scale bar is 100 μm .

Janus porous aluminum mesh by a combination of fluorosilane modification and femtosecond laser drilling, which had also contributed to the deep understanding of a Janus system for UGB unidirectional transport.^[12] Though these previous explorations have greatly advanced the experimental and theoretical guidance for manipulating UGBs, several drawbacks arise subsequently. 1) Fabricating methods for a classical Janus architecture by chemical etching or fluorination are so tedious and not environment-benign.^[9–12] 2) Surface wettability modification by oxygen plasma tends to be unstable for maintaining the Janus performance because the low molecular weight chains diffuse from the PDMS and cover up the thermodynamically unstable surface.^[10,13] 3) Achieving the switchable unidirectional passage and double-faced blockage for UGBs, that is, reversible dynamic control between Janus and non-Janus system, by a single Janus membrane has rare investigations. In this view, developing a more facile, environment-friendly and reliable stimuli-responsive Janus membrane with dynamically reversible wettability is a potential need.

Herein, we report a dual UV/thermal-responsive Janus underwater air bubble “diode” on the basis of a single TAZF

which was fabricated by one-step laser drilling and a subsequent heating process (Heat-TAZF). In aqueous medium, the resultant Heat-TAZF allows the passage of UGB marching from an aerophobic (AB) surface toward an aerophilic (AL) surface with an ultrashort period of 0.5 s, whereas it repels the UGBs from passing through in an opposite direction (Figure S1 and Movie S1, Supporting Information). Significantly, the reversible switching between double-faced AB and recovery Janus architecture could be readily achieved by virtue of alternant UV-irradiation (UV-TAZF) and re-heating (Re-Heat-TAZF) dispositions, that is, the reversible conversion between double-faced repelling and unidirectional transport of UGBs. The underlying mechanism revealed by X-ray photoelectron spectroscopy (XPS) spectrums is that the reversible graft and removal of hydroxyl (–OH) on top surface of UV-TAZF and Re-Heat-TAZF dominates the wettability conversion. Additionally, the quantitative relationship among the UV and heating time and the water contact angle (WCA) and the UGBCA has been systematically studied. This work provides insights for guiding researchers to achieve the controllable manipulation of gas bubbles in aqueous media,

and extends the application of UV/thermal-responsive Janus membrane with tunable wettability.

Figure 1a shows the wettability tuning strategy for an air bubble “diode.” First, one-step laser drilling was utilized for fabricating a single non-Janus TAZF with top/bottom diameter, WCA and UGBCA of 141/60 μm , 0°/30°, and 150°/136°, respectively. This TAZF exhibited double-faced repelling UGBs (Figure 1b–d). Once it was subjected to a heating process, the Heat-TAZF had been dramatically modified to a Janus performance, the corresponding top/bottom WCA and UGBCA of which were modified to 154°/79° and 29°/111°, respectively. This resultant Heat-TAZF was then carried out for investigating the penetration behavior of UGBs. As shown in Figure 1e,f, the underwater bubble was inclined to permeate from AB surface to AL surface, whereas the bubble tended to be blocked in an opposite direction (Movie S2, Supporting Information). Exposed to UV-irradiation, the TAZF was then modified to a non-Janus membrane for double-faced repelling UGBs once more and the measured top/bottom WCA and UGBCA for UV-TAZF changed to 33°/61° and 148°/116°, respectively. On this basis, another re-heating operation imparted the remedy of Janus TAZF with top/bottom WCA and UGBCA of 150°/68° and 38°/125° (Figure S2, Supporting Information), signifying that the dynamic conversion between Janus and non-Janus property could be readily realized by alternative thermal/UV treatment. Notably, the change amplitude of wettability on the top surface of TAZF is far larger than a bottom one, which should be attributed to the relatively sufficient roughness, specific surface area, and –OH attaching sites on top surface compared to a bottom one (Figure S3, Supporting Information). For UV treatment, the much rougher top surface enabled more abundant

–OH adsorption than a flat bottom one, which thus led that the hydrophilic wettability (WCA = 30°) for top surface is better than that (WCA = 61°) for bottom one. For heat treatment, the desorption of –OH had been achieved on both the top and bottom surfaces. While the rougher top surface imparted the more active entrance of air so as to harvest a super-hydrophobic Cassie mode in comparison with a flat bottom surface with a hydrophilic Wenzel mode. So, the dynamic conversion between Janus and non-Janus system should be dominated by the top rough surface of TAZF.

The mechanism for the reversible conversion of wettability via UV light and heating was systemically investigated. Convincingly, the conversion of the chemical functional groups on material’s surface is recognized as the main reason,^[14] which contributes to the dynamic interconversion between adsorption and desorption of hydroxyl groups (Figure 2a). For clarity, typical XPS spectrums were carried out for monitoring the content variation of oxygen atom on the top surface of four-state TAZF (Figure S4, Supporting Information). Accordingly, peak-differentiating and imitating had been successfully conducted to the raw XPS spectrums of oxygen atom, where the peaks located at 530.4 and 532.0 eV should be assigned to the binding energy of Zn-O and Zn-OH (Figure 2b–e), respectively.^[15] As shown in Figure 2f, (1) once the pristine TAZF was heated, the relative content of Zn-OH decreased sharply from 83.2% to 48.0%, while Zn-O had increased from 16.8% to 52.0%, which indicates that the top surface of TAZF had realized a conversion from hydrophilic to hydrophobic performance. 2) Once the Heat-TAZF suffered from UV-irradiation, the relative content of Zn-OH increased slightly from 48.0% to 55.2% in contrast to that of Zn-O decreased from 52.0% to 44.8%,

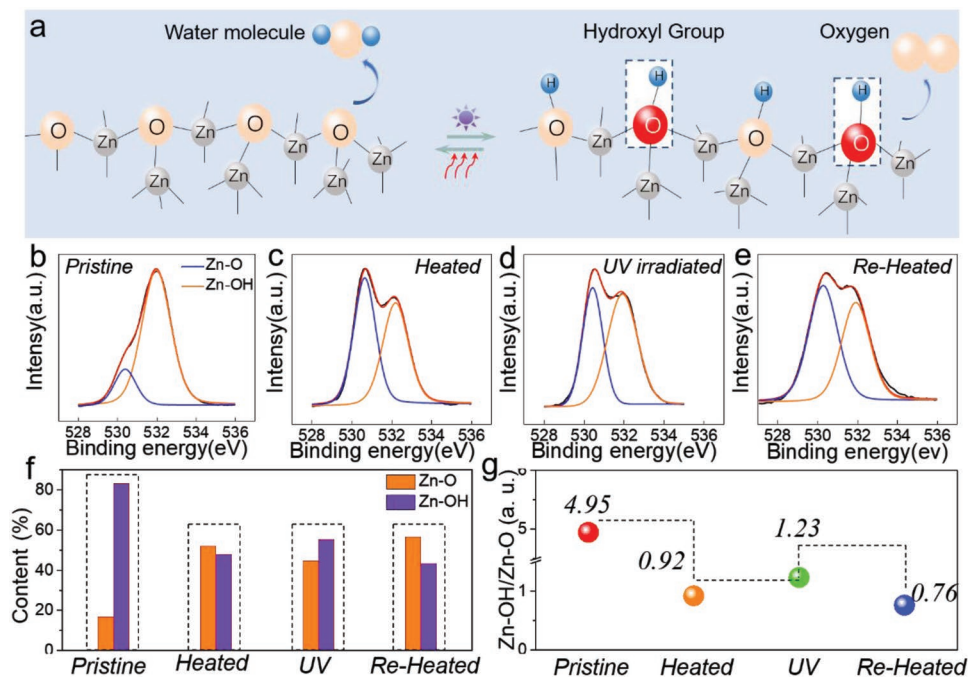


Figure 2. a) Schematic mechanism for the wettability reversible conversion between hydrophilicity and hydrophobicity by applying alternative UV and temperature triggers on top surface of TAZF. XPS spectrums for the observation of O1s peak’s evolution on top surfaces of b) TAZF, c) Heat-TAZF, d) UV-TAZF, and e) Re-Heat-TAZF, respectively. f,g) Comparison for the relative content of Zn-O and Zn-OH on top surfaces of TAZF, Heat-TAZF, UV-TAZF, and Re-Heat-TAZF, respectively.

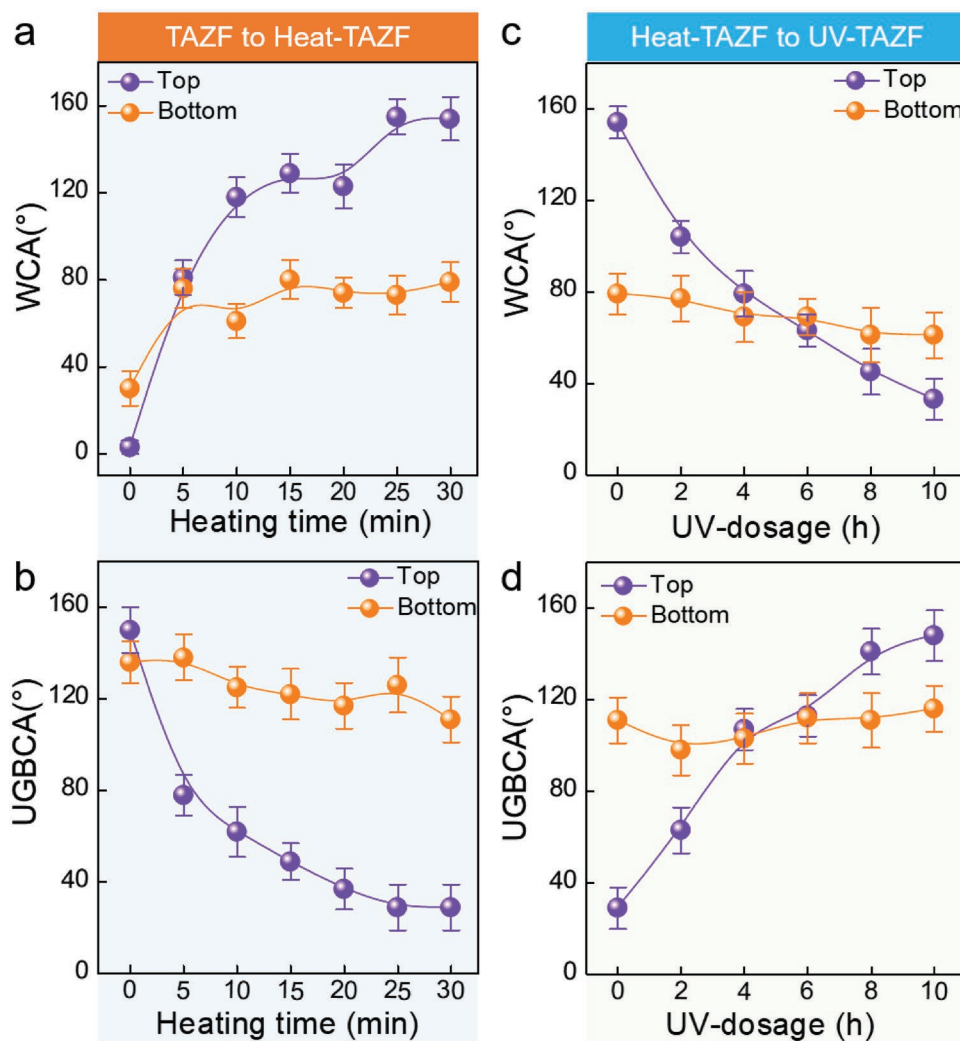


Figure 3. (a) and (b) show the evolution of WCA with UV-light and heating time, respectively. (c) and (d) show the evolution of BCA with UV-light and heating time, respectively.

which indicates that the successful graft of hydroxyl group endowed the TAZF with a hydrophilic property once more.^[16] 3) Once the TAZF was subsequently reheated, the relative content of Zn-OH decreased slightly from 55.2% to 43.3% in comparison with that of Zn-O increased from 44.8% to 56.7%, which indicates that the discharge of hydroxyl group contributes to a hydrophobic top surface.^[17] In addition, the relative ratio of Zn-OH and Zn-O also demonstrated that the reversible dynamic control between Janus and non-Janus TAZF could be readily achieved by applying alternative thermal/UV treatment (Figure 2g). Since the surface chemical compositions is highly dependent on UV and heating time, we also explored the effect of heating time and UV irradiation time on the WCA and UGBCA for top/bottom surface of TAZF. **Figure 3a** shows the WCA and UGBCA variation as a function of heating time, where we could detect that the WCA of top surface increased exponentially with the elevation of heating time when the WCA reached its plateau at 25 min and stabilized at 155°. Simultaneously, the WCA of bottom surface tend to achieve its maximum of 80° within 15 min and there was no change even though

more heating time was supplied. It is well known that the theoretical WCA and UGBCA should be supplementary angle,^[10] which was also demonstrated in our experimental measurements (Figure 3b). The measured UGBCA for the top surface decreases exponentially from 150° to 31° within 25 min heating time, whereas the UGBCA of the bottom surface tended to decrease from 145° to a constant 111° within 15 min heating time. Accordingly, the heating time of 25 min was selected as an optimized thermal-heating condition for harvesting a Janus Heat-TAZF. In sharp contrary, non-Janus UV-TAZF could be donated from the elevation of UV-irradiation time by virtue of the graft of hydroxyl group. Figure 3c,d revealed the wettability recovery process under the aid of UV-irradiation. Apparently, the WCA of top surface decreases sharply from 156° to 30° within 9 h UV-irradiation, whereas it was decreased slightly from 79° to 61° for the bottom surface (Figure 3c). In comparison, the double-faced AL performance was recovered for a non-Janus UV-TAZF within 4 h (Figure 3d). Though the time-consuming treatment in terms of UV-irradiation is comparatively inefficient, some improvements such as elevating

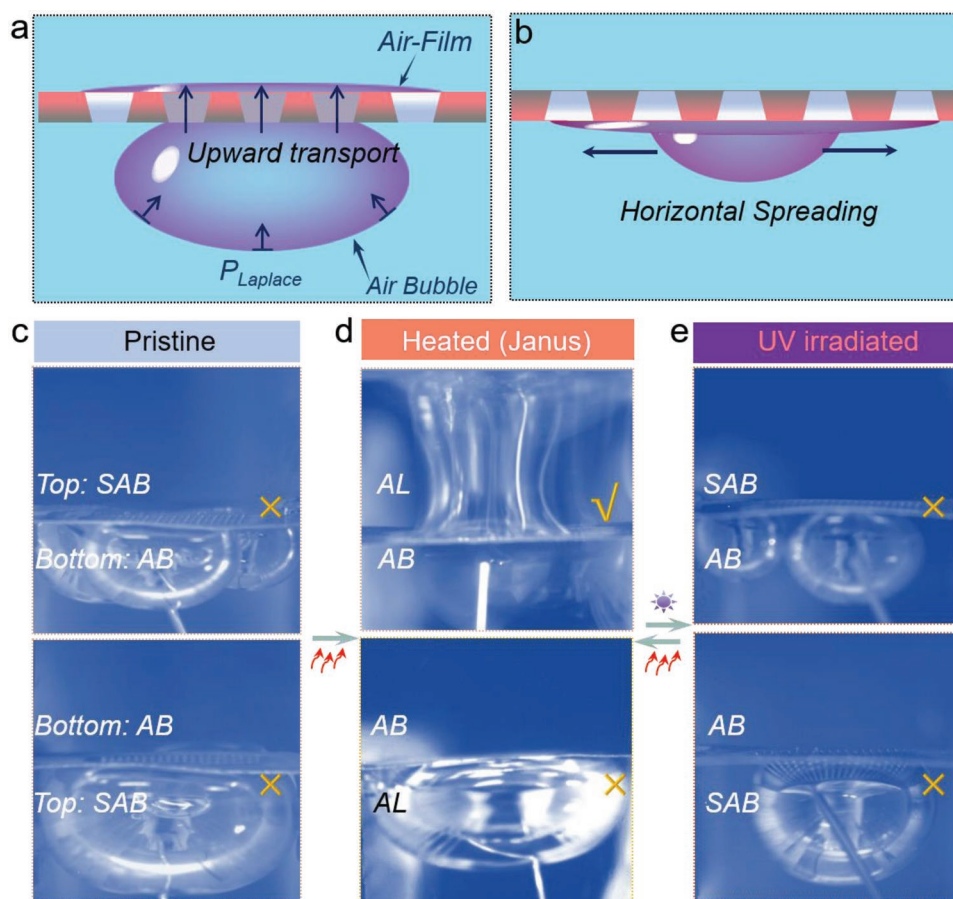


Figure 4. a,b) The schematic of the mechanism of the bubble unidirectional transport on Heat-TAZF. c–e) In situ observation of dynamic behavior of bubble on the TAZF, Heat-TAZF, UV-TAZF, respectively.

the light power intensity^[18] and utilizing alcohol-assisted UV irradiation method^[19] are convinced to further shorten its corresponding time scale. In short, the result indicates the top surface is much more sensitive to UV/thermal-stimulus in comparison with a bottom one of TAZF. This verified that a rough top morphology subjected to much more severe laser ablation should possess much larger specific surface area and more hydroxyl group attaching sites than a flat bottom one. So, the reversible conversion between Cassie model and Wenzel model on top surface of Heat-TAZF and UV-TAZF could be realized by alternately applying a thermal or UV stimuli on-demand (Figure S5, Supporting Information). In addition, the durability test was conducted and the result verified that current Janus TAZF had good wettability stability for at least 1 month (Figure S6, Supporting Information). Thus, the reversible conversion between Janus (AL top surface and AB bottom surface) and non-Janus (SAB top surface and AB bottom surface) TAZF could be readily achieved by selectively applying a thermal/UV-trigger. Utilizing a TAZF with the optimized heating and UV-irradiation time, the reversible control between double-faced repelling UGBs and unidirectional self-transport of UGBs were demonstrated. As shown in **Figure 4c**, the original non-Janus TAZF exhibited double-faced blockage for UGB due to the absence of a giant wettability gradient force ($F_{\text{wet-grad}}$). Once it was subjected to heating treatment, the enormous wettability

change on top surface allowed the formation of Janus Heat-TAZF with a giant $F_{\text{wet-grad}}$, which had greatly endowed the gas bubbles in aqueous media with unidirectional self-transport property (Figure 4d). Thereafter, Janus Heat-TAZF can recover to a non-Janus UV-TAZF for double-faced repelling UGBs by UV-irradiation (Figure 4e and Movie S3, Supporting Information). Additionally, the underlying mechanism for UGB unidirectional transport dependent on a Janus Heat-TAZF could be revealed according to a classical equation^[20]

$$P_{\text{Laplace}} = \gamma \left(\frac{1}{R_1} - \frac{1}{R_2} \right) \quad (1)$$

where γ is the surface tension of water ($7.2 \times 10^{-2} \text{ N m}^{-1}$), R_1 is the radius of curvature for UGB, and R_2 represents the radius of curvature for the air film. Accordingly, the injected UGBs tended to penetrate from an AB surface to an AL surface because of an upward P_{Laplace} ($R_2 \gg R_1$) indicated by Equation (1) (Figure 4a). In contrast, the UGBs would be repelled in an opposite direction when P_{Laplace} was too small to overcome an intrusion pressure deriving from water resistance (Figure 4b).

In summary, a dual UV/thermal-responsive Janus underwater gas bubble “diode” on the basis of a single TAZF has been fabricated by combining one-step laser drilling and a subsequent heating process. In aqueous medium, the resultant

Heat-TAZF allows the penetration of UGB from an AB surface toward an AL surface within an ultrashort period of 0.5 s, whereas it would block the UGBs from passing through in an opposite direction. Moreover, the reversible switching between double-faced AB and Janus architecture could be easily achieved by virtue of alternant UV-irradiation and heating dispositions, that is, the reversible conversion between double-faced repelling and unidirectional transport of UGBs. The underlying mechanism clarified by XPS spectrums is that the reversible graft and removal of hydroxyl group on top surface of UV-TAZF and Heat-TAZF dominates the wettability conversion. Additionally, the quantitative relationship among the UV and heating time and the WCA and the UGBCA has been systematically investigated. Significantly, the top rough topography with more specific surface area and hydroxyl groups attaching sites has been demonstrated a dominant factor in determining the wettability variation of TAZF in comparison with a flat bottom one. The current fabrication process of the Janus system is more facile, time-saving, and environment-benign, which is expected to provide new insight for the design of synergetic light/thermal-responsive surfaces for applications in ultrafast bubble capture, transportation, collection, and gas/liquid separation.

Experimental Section

Nanosecond Laser Fabrication: The Zn foil (99.5% purity, 50 μm thick) was purchased from New Metal Material Tech. Co., Ltd., Beijing, China. The uniform conical micropore arrays with a space of 200 μm were drilled by using a frequency-tripled, Q-switched, single-mode neodymium doped yttrium aluminum garnet nanosecond laser (Spectra-Physics) with 355 nm wavelength, 10 Hz repetition rate, 10 ns pulse width, and 50 mw laser power.

Switchable Wettability Strategy: The TAZF wrapped with opaque tin foil was heated for 30 min at 250 $^{\circ}\text{C}$ on a heating plate (Lab Tech, EH35A plus). For UV light irradiation, a 70 W UV LED lamp with a wavelength of 365 nm was placed above the top surface of TAZF at a distance about 2 cm as the light source.

Characterization: The surface morphology was characterized by using a field-emission scanning electron microscope (Hitachi S-4800, Japan). Surface roughness, 3D image, and cross-sectional profile were measured by using a WYKO noncontacting optical profiling microscope. The contact angles of the water droplet and underwater gas bubble were measured using a CA100C contact-angle system (Innuo, China) with the sessile drop method. The average values were obtained by measuring five drops at different locations on the same surface. All the contact angle measurements were conducted at 10% humidity and 20 $^{\circ}\text{C}$ temperature. A high-speed (FASTCAM SA6, Photron, USA) camera was used to record the time that underwater bubbles (40 μL) penetrate from the AB surface to the AL surface on the Heat-TAZF. The high-speed videos were taken using a typical rate of 6400 frames s^{-1} and shutter speed of 1/200 000 s.

Underwater Bubble Unidirectional Penetration Test: Putting a homemade glass rack in plastic container filled with deionized (DI) water (40 mL) and fix the objective TAZF on it. The underwater bubbles were continuously provided by an injection syringe below the TAZF. Photos were taken continuously using a computer-controlled charge-coupled device camera to show the real-time images of the bubbles on TAZF.

Supporting Information

Supporting Information is available from the Wiley Online Library or from the author.

Acknowledgements

This work was supported by the National Natural Science Foundation of China (Nos. 51875160, 51805508, 61505047, 51875544, and 61805230), Fundamental Research Funds for the Central Universities (No. WK2090090024), China Postdoctoral Science Foundation (No. BH2090000025).

Conflict of Interest

The authors declare no conflict of interest.

Keywords

air diodes, Janus membranes, laser drilling, light/temperature-responsive, reversible wettability

Received: July 8, 2019

Revised: August 7, 2019

Published online:

- [1] a) A. Khalil, S. A. El-Agouz, Y. A. F. El-Samadony, A. Abdo, *Desalination* **2015**, 372, 7; b) H. M. Abd-Ur-Rehman, F. A. Al-Sulaiman, *Energy Convers. Manage.* **2016**, 127, 667.
- [2] a) U. V. Gunten, *Water Res.* **2003**, 37, 1443; b) E. Forgacs, T. Cserhati, G. Oros, *Environ. Int.* **2004**, 30, 953.
- [3] M. S. K. A. Sarkar, S. W. Donne, G. M. Evans, *Adv. Powder Technol.* **2010**, 21, 412.
- [4] a) M. B. Kermani, A. Morshed, *Corrosion* **2003**, 59, 659; b) A. Samimi, *Int. J. Sci. Eng. Invent.* **2012**, 1, 32.
- [5] a) A. V. Soloviev, P. Schlussel, *J. Phys. Oceanogr.* **1994**, 24, 1339; b) J. Gylys, T. Zdankus, M. Gylys, *Int. J. Heat Mass Transfer* **2014**, 69, 230.
- [6] L. D. Temmerman, T. Maere, H. Temmink, A. Zwijnenburg, I. Nopens, *Water Res.* **2015**, 76, 99.
- [7] a) J. Ju, H. Bai, Y. Zheng, T. Zhao, R. Fang, L. Jiang, *Nat. Commun.* **2012**, 3, 1247; b) X. Tian, H. Jin, J. Sainio, R. H. Ras, O. Ikkala, *Adv. Funct. Mater.* **2014**, 24, 6023; c) H. Li, M. Cao, X. Ma, Y. Zhang, X. Jin, K. Liu, L. Jiang, *Adv. Mater. Interfaces* **2016**, 3, 1600276; d) Y. Zhao, H. Wang, H. Zhou, T. Lin, *Small* **2017**, 13, 1601070. e) H. C. Yang, Y. Xie, J. Hou, A. K. Cheetham, V. Chen, S. B. Darling, *Adv. Mater.* **2018**, 30, 1801495.
- [8] a) H. Yang, J. Hou, L. Wan, V. Chen, Z. Xu, *Adv. Mater. Interfaces* **2016**, 3, 1500774; b) K. Yin, S. Yang, X. R. Dong, D. Chu, J.-A. Duan, J. He, *Appl. Phys. Lett.* **2018**, 112, 243701; c) R. Waldman, H. Yang, D. J. Mandia, P. F. Nealey, J. W. Elam, S. B. Darling, *Adv. Mater. Interfaces* **2018**, 5, 1800658. d) C. Chen, L.-A. Shi, Z. Huang, Y. Hu, S. Wu, J. Li, D. Wu, J. Chu, *Adv. Mater. Interfaces* **2019**, 6, 1900297.
- [9] J. Chen, Y. Liu, D. Guo, M. Cao, L. Jiang, *Chem. Commun.* **2015**, 51, 11872.
- [10] J. Yong, F. Chen, J. Huo, Y. Fang, Q. Yang, J. Zhang, X. Hou, *Nanoscale* **2018**, 10, 3688.
- [11] C. Pei, Y. Peng, Y. Zhang, D. Tian, K. Liu, L. Jiang, *ACS Nano* **2018**, 12, 5489.
- [12] S. Yan, F. Ren, C. Li, Y. Jiao, C. Wang, S. Wu, S. Wei, Y. Hu, J. Li, Y. Xiao, Y. Su, D. Wu, *Appl. Phys. Lett.* **2018**, 113, 261602.
- [13] a) D. Bodas, C. Khan-Malek, *Sens. Actuators, B* **2007**, 123, 368; b) B. D. Silva, M. Zhang, G. Schelcher, L. Winter, C. Guyon, P. Tabeling, D. Bonn, M. Tatoulian, *Plasma Processes Polym.* **2017**, 14, 1600034.
- [14] H. Hu, H. F. Ji, Y. Sun, *Phys. Chem. Chem. Phys.* **2013**, 15, 16557.

- [15] a) A. L. Armelao, F. M. Fabrizio, G. S. Gialanella, Z. F. Zordan, *Thin Solid Films* **2001**, 394, 89; b) D. Pradhan, K. T. Leung, *J. Phys. Chem. C* **2008**, 112, 1357.
- [16] a) D. Wang, Y. Liu, X. Liu, F. Zhou, W. Liu, Q. Xue, *Chem. Commun.* **2009**, 7018; b) V. Khranovskyy, T. Ekblad, R. Yakimova, L. Hultman, *Appl. Surf. Sci.* **2012**, 258, 8146; c) H. Wang, Z. Guo, *Appl. Phys. Lett.* **2014**, 104, 183703; d) J. Yong, F. Chen, Q. Yang, Y. Fang, J. Huo, X. Hou, *Chem. Commun.* **2015**, 51, 9813.
- [17] a) L. Yang, Q. Zhao, M. Willander, X. Liu, M. Fahlman, J. Yang, *Appl. Surf. Sci.* **2010**, 256, 3592; b) D. F. Zhao, R. Jia, N. K. Gao, W. S. Yan, L. Zhang, X. Li, D. Liu, *J. Phys. Chem. C* **2017**, 121, 12745.
- [18] Y. Jiao, C. Li, S. Wu, Y. Hu, J. Li, L. Yang, D. Wu, J. Chu, *ACS Appl. Mater. Interfaces* **2018**, 10, 16867.
- [19] a) R. Wang, N. Sakai, A. Fujishima, T. Watanabe, K. Hashimoto, *J. Phys. Chem. B* **1999**, 103, 2188; b) D. Tian, X. Zhang, Y. Tian, Y. Wu, X. Wang, J. Zhai, L. Jiang, *J. Mater. Chem.* **2012**, 22, 19652.
- [20] a) X. Ma, M. Cao, C. Teng, H. Li, J. Xiao, K. Liu, L. Jiang, *J. Mater. Chem. A* **2015**, 3, 15540; b) C. Zhang, B. Zhang, H. Ma, Z. Li, X. Xiao, Y. Zhang, X. Cui, C. Yu, M. Cao, L. Jiang, *ACS Nano* **2018**, 12, 2048.